

DYNAMIC ANALYSIS OF AEROELASTIC RESPONSE FOR TRANSONIC FLOW WITH NONLINEAR STRUCTURAL MODEL

E. Camilo*, F. D. Marques*, J. L. F. Azevedo**

***Universidade de São Paulo, São Carlos, SP, 13566-590, BRAZIL**

****Instituto de Aeronáutica e Espaço, São José dos Campos, SP, 12228-903, BRAZIL**

Keywords: *Aeroelasticity, nonlinear dynamics, limit cycle oscillations, transonic flow*

Abstract

The present paper is concerned with dynamic analysis of time marching aeroelastic responses of typical sections in transonic flow with nonlinear structural models. An aeroelastic model is proposed in which the concentrated nonlinearities can be described by continuous functions, namely using hyperbolic tangent and polynomial functions. Typical free-play described by continuous functions is also adopted. Major interest is in verifying how the degree of the structural nonlinearity affects the transonic aeroelastic behavior. An Euler CFD code based on the finite volume discretization for unstructured grids is used for the unsteady aerodynamic loading assessment. The results shown in the paper are particularly concerned with the investigation of nonlinear effects for transonic flow over a NACA 0012 airfoil-based typical section. The investigation considers both time histories of the aeroelastic response as well as phase plane analyses.

1 Introduction

In the last decade, nonlinear dynamic analysis developed quickly, both from a theoretical and an experimental point of view, in a vast diversity of fields in science and engineering. However, most aeroelastic analyses of flight vehicles are performed under the assumption of linearity. Under this assumption, the characteristics of flutter and divergence can be obtained using well-

established tools. On the other hand, the influence of nonlinearities on modern aircraft is becoming increasingly important and the need for more accurate predictive tools grows stronger.

Nonlinear aeroelastic stability and response analysis has evolved, mainly due to advances in computational tools. Computational aeroelasticity is a relatively new field emphasizing those types of aeroelastic problems where loads based on Computational Fluid Dynamics (CFD) methods, which can be both unsteady and nonlinear, are used [1, 2, 3]. A significant amount of effort devoted toward the numerical solution of transonic aeroelastic phenomena, not only in the prediction of transonic dip effects [4, 5, 6], but also toward that of limit cycle oscillations (LCOs). Euler and Navier-Stokes schemes have been coupled with structural models [7, 8].

The nonlinearities in aeroelastic analyses are divided into aerodynamic and structural ones. In this paper, the aerodynamic nonlinearities arise from the presence of shock waves in transonic flows. For such flow conditions, the unsteady forces generated by the motion of the shock waves have been shown to destabilize the airfoil pitching motion and affect the bending-torsional flutter condition by lowering the flutter speed in the so-called transonic dip phenomenon. Structural nonlinearities can also lead to LCO whether the flow is transonic or not. However, the present understanding of LCO induced by aerodynamic nonlinearities is less complete, and no systematic

quantitative correlation between theory and experiment has been achieved [9].

Structural nonlinearities can be classified as distributed or concentrated. The distributed nonlinearities are spread over the entire structure and can manifest itself through complex material behavior, by aging effects, and due to faulty joints, junctions, or links. The concentrated nonlinearities are those acting locally, being basically assumed for simplified structural models. Studies with concentrated nonlinearities have revealed significant effects on the aeroelastic stability, allowing the presence of chaotic motion and limit cycle oscillation below the flutter speed [10, 11]. Although it is noticed the effects on aeroelastic stability of combined aero-structural nonlinearities, more effort in modelling such problem is necessary. It has been also observed the need for deeper understanding of aeroelastic mechanisms due to severe nonlinearities.

Free-play nonlinearities occur in the control surfaces or components with loose joints [12]. The amount of free-play within the system is usually small. Although the structural motion is relatively small, the effect of fatigue on the structure is highly problematic. The conventional method for studying limit cycles is to perform numerous simulations using Runge-Kutta time integrations. The accuracy of these runs, for free-play, depends on particularly methods to treat discontinuities [13, 14]. On the other hand, works have been described structural nonlinearities in terms of continuous functions, even to represent free-play [15].

The aim of this paper is to investigate the dynamics behavior of typical section with continuous structural nonlinearities in transonic regime. The modelling methodology is based on coupling typical section motion equations to an Euler unsteady CFD code to obtain time marching aeroelastic responses and phase plane through the fourth-order Runge-Kutta scheme [7, 8]. In order to solve the aerodynamic problem, the Euler equations are integrated by a finite volume discretization on unstructured grids [16]. Concentrated structural nonlinearities are introduced to the model by means of functions of the restor-

ing moment *versus* the angle of incidence of the airfoil. In this way, it has been considered concentrated nonlinearities described by continuous functions form, in terms of hyperbolic tangent and polynomial functions. Typical free-play described by continuous and discontinuous functions are also adopted. The results are, then, presented to illustrate the influence of structural nonlinearity degree in the aeroelastic behavior in transonic flow.

2 Aerodynamic Model

In the present study, the flow is assumed to be governed by the two-dimensional, time-dependent Euler equations, which may be written in conservative form and Cartesian coordinates as

$$\frac{\partial}{\partial t} \int_V \mathbf{Q} dx dy + \int_S (\mathbf{E} dy - \mathbf{F} dx) = 0, \quad (1)$$

where \mathbf{V} represents the area of the control volume and \mathbf{S} is its boundary, \mathbf{Q} is the vector of conserved quantities and the inviscid flux vectors, \mathbf{E} and \mathbf{F} , are given by

$$\mathbf{Q} = \begin{bmatrix} \rho \\ \rho u \\ \rho v \\ e \end{bmatrix}, \quad \mathbf{E} = \begin{bmatrix} \rho U \\ \rho u U + p \\ \rho v U \\ (e + p)U + x_t p \end{bmatrix},$$

$$\mathbf{F} = \begin{bmatrix} \rho V \\ \rho V u \\ \rho V v + p \\ (e + p)V + y_t p \end{bmatrix}, \quad (2)$$

where ρ , u , v , p and e are density, Cartesian components of the velocity, pressure, and specific energy, respectively. U and V are Contravariant velocity components, defined as

$$U = u - x_t, \quad V = v - y_t, \quad (3)$$

where x_t and y_t represents the Cartesian velocity components of the mesh.

The Euler equations can be rewritten for each i -th control volume as

$$\frac{\partial}{\partial t} (V_i \mathbf{Q}_i) + \int_{S_i} (\mathbf{E} dy - \mathbf{F} dx) = 0. \quad (4)$$

The 2-D Euler equations are discretized by a finite volume procedure in an unstructured mesh. The equations are discretized in space by a centered scheme, together with added artificial dissipation terms. The artificial dissipation operator, D_i , can be written as

$$D_i = d^2(\mathbf{Q}_i) - d^4(\mathbf{Q}_i), \quad (5)$$

where $d^2(\mathbf{Q}_i)$ represents the contribution of the undivided Laplacian operator, and $d^4(\mathbf{Q}_i)$ is the contribution of the biharmonic operator [17]. The biharmonic operator is responsible for providing the background dissipation to damp high frequency uncoupled error modes and the undivided Laplacian artificial dissipation operator prevents oscillations near shock waves. The Euler solver is integrated in time by a second-order accurate, 5-stage, explicit, Runge-Kutta time-stepping scheme, as presented in [1].

3 Aeroelastic Equations

The physical model considered in the present work is a typical section with pitch and plunge degrees of freedom and free of mechanical friction [18]. The equations of motion of this aeroelastic system, with a linear structure, can be written in the form

$$\frac{d\mathbf{w}_s}{dt} = \mathbf{R}_s, \quad (6)$$

where

$$\mathbf{R}_s = \left[\begin{array}{cccc} 1 & 0 & 0 & 0 \\ 0 & 1 & 0 & \frac{1}{2}x_\alpha \\ 0 & 0 & 1 & 0 \\ 0 & x_\alpha & 0 & \frac{1}{2}r_\alpha^2 \end{array} \right]^{-1} \left\{ \begin{array}{l} \left[\begin{array}{cccc} 0 & & & \\ & (2/\mu_s\pi)C_l & & \\ & 0 & & \\ & & (4/\mu_s\pi)C_m & \end{array} \right] \\ - \left[\begin{array}{cccc} 0 & -1 & 0 & 0 \\ (2\omega_R/\bar{U})^2 & 0 & 0 & 0 \\ 0 & 0 & 0 & -1 \\ 0 & 0 & 2r_\alpha^2/(\bar{U})^2 & 0 \end{array} \right] \mathbf{w}_s \end{array} \right\} \quad (7)$$

and $\mathbf{w}_s = [h, \dot{h}, \alpha, \dot{\alpha}]^T$. In the previous equation, h is the plunge linear displacement and α is the incidence, or pitch angular displacement. Here, $r_\alpha = \sqrt{I_\alpha/m}$ is the radius of gyration defined in terms of the pitch moment of inertia I_α and

the airfoil mass per unit span m , x_α is the offset between the center of mass and the elastic axis, $\mu_s = m/\pi\rho_\infty b^2$ is the airfoil-to-fluid mass ratio defined in terms of the fluid freestream density ρ_∞ and the semi-chord, b . Moreover, $\omega_R = \frac{\omega_h}{\omega_\alpha}$ is the ratio of the natural frequencies of plunging (ω_h) and pitching (ω_α), $\bar{U} = \frac{U_\infty}{b\omega_\alpha}$ is the reduced velocity defined in terms of the fluid freestream velocity U_∞ , and C_l and C_m are the lift and moment coefficients about the elastic axis, respectively.

The fourth-order Runge-Kutta time stepping scheme is used for the time marching aeroelastic analyses. Time integration of the coupled fluid-structural equations of motion (Eq. (7)) is incorporated within the CFD Euler code as follows:

1. At time level n , perform an iteration of the Euler equation and calculate values for C_l and C_m ;
2. This information is used by the equations of motion to determine the position and velocity of the airfoil through the fourth-order Runge-Kutta scheme;
3. The aerodynamic mesh is moved to a new position and velocity of the airfoil and the process is repeated.

4 Torsional Structural Nonlinearity

Several classes of nonlinear stiffness contributions have been studied in papers treating the open-loop dynamics of the aeroelastic system [19]. In this work, the linear torsional moment function is replaced by the nonlinear function

$$\bar{M}(\alpha) = \bar{K}_\alpha \alpha = K_\alpha f(\alpha), \quad (8)$$

where K_α is considered as a global stiffness. The functional form of $f(\alpha)$ can be expressed as a polynomial nonlinearity for restoring torsion

$$f(\alpha) = f_{\alpha_0} + f_{\alpha_1} \alpha + f_{\alpha_2} \alpha^2 + \dots + f_{\alpha_n} \alpha^n. \quad (9)$$

Combination of hyperbolic tangent functions to represent polynomial nonlinearity is also proposed here [15]. This approach provides an easier

way to produce variations to the functions governing the nonlinear torsional behavior. Therefore, the representation for torsion by means of hyperbolic tangent functions is

$$f(\alpha) = \frac{1}{2} [1 - \tanh(\varepsilon(\alpha - \alpha_-))] (\alpha - \alpha_-) + \frac{1}{2} [1 + \tanh(\varepsilon(\alpha - \alpha_+))] (\alpha - \alpha_+), \quad (10)$$

where α_- and α_+ are the lower and upper boundaries, respectively, to be adjusted depending on the nonlinear behavior range in terms of incidence angle, and ε is a variable that determines the intensity of the function shape.

The free-play model is relatively simple and considers that any pitching displacement between a range of α_- and α_+ of the incidence angle would result in no structural restoring reaction. The $f(\alpha)$ function for the free-play case is given by

$$\begin{cases} f(\alpha) = \alpha - \alpha_+ & \text{for } \alpha > \alpha_+ \\ f(\alpha) = 0 & \text{for } \alpha_- \leq \alpha \leq \alpha_+ \\ f(\alpha) = \alpha - \alpha_- & \text{for } \alpha < \alpha_- \end{cases} \quad (11)$$

Discontinuous free-play nonlinearity has been normally utilized to represent loose hinges or linkages backlash of control surfaces and for nonlinear aeroelastic behavior analyses [8, 10]. Previous details on smooth nonlinear function shapes for torsional restoring structural moments have shown that hyperbolic tangent functions can be easily modified to cover from linear to extreme shapes similar to discontinuous forms. For instance, in the Fig. 1 is illustrated hyperbolic tangent function for a particular choice of α_- and α_+ boundaries and increasing ε . Here, the discontinuous free-play representation (Eq. (11)) in the model is used to compare aeroelastic behavior with continuous free-play representation (Eq. (10)).

5 Time-Marching Aeroelastic Analysis

The results for the time marching method have been studied through the time histories of the solution and through phase plane analyses. The pa-

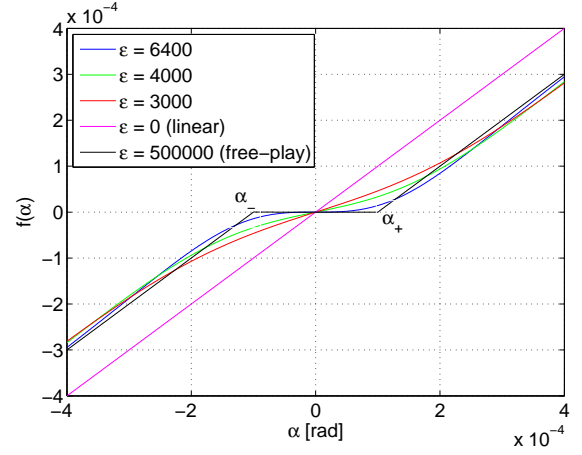


Fig. 1 Restoring moment in torsion as \tanh functions of α .

rameters for the structural model are given in Table 1. The results were calculated by first computing a converged steady flow solution about the airfoil with angle 0.5 degree of pitching about the elastic axis. The steady Euler solution was determined using the steady portion of the original unsteady Euler solver. Then, the coupled computational fluid dynamic (CFD) and computational structural dynamics (CSD) method to the two-dimensional typical section was performed. It consists of a NACA0012 airfoil.

Table 1 Structural model parameters.

Parameter	Value
r_α	0.539
x_α	-0.2
ω_R	0.343
μ_s	100.0
x_{ea}	-0.1
y_{ea}	0.0

Time marching analyses including torsional polynomial and hyperbolic tangent nonlinearities in the structure have been calculated. Torsional polynomial nonlinearities are added according to type and incidence considered in the model. For all cases previously analyzed, one can observe that the LCO amplitudes, with parameter model given in Table 1, typically involve very small in-

cidences. As a form of further evaluating the analysis procedure implemented, three types of polynomial nonlinearities are added to the model. These are classified according to the degree of the polynomial, and the same incidence interval is considered, as indicated in Fig. 2.

The first structural nonlinearity is a 7-degree polynomial, P7, given by

$$f(\alpha) = (3.672 \times 10^{-1})\alpha - (2.838 \times 10^{-12})\alpha^2 + (3.440 \times 10^6)\alpha^3 + (1.285 \times 10^{-5})\alpha^4 - (8.191 \times 10^{12})\alpha^5 - (1.769 \times 10)\alpha^6 + (6.440 \times 10^{18})\alpha^7. \quad (12)$$

The second structural nonlinearity is a 11-degree polynomial, P11, given by

$$f(\alpha) = (1.307 \times 10^{-1})\alpha - (2.321 \times 10^{-11})\alpha^2 + (1.006 \times 10^7)\alpha^3 + (3.348 \times 10^{-4})\alpha^4 - (6.081 \times 10^{13})\alpha^5 - (1.677 \times 10^3)\alpha^6 + (1.785 \times 10^{20})\alpha^7 + (3.399 \times 10^9)\alpha^8 - (2.480 \times 10^{26})\alpha^9 - (2.437 \times 10^{15})\alpha^{10} + (1.307 \times 10^{32})\alpha^{11}. \quad (13)$$

Finally, the third structural nonlinearity is a 13-degree polynomial, P13, given by

$$f(\alpha) = (3.579 \times 10^{-2})\alpha + (7.940 \times 10^{-10})\alpha^2 + (1.451 \times 10^7)\alpha^3 - (1.752 \times 10^{-2})\alpha^4 - (1.197 \times 10^{14})\alpha^5 + (1.384 \times 10^5)\alpha^6 + (5.116 \times 10^{20})\alpha^7 - (4.861 \times 10^{11})\alpha^8 - (1.157 \times 10^{27})\alpha^9 + (7.757 \times 10^{17})\alpha^{10} + (1.317 \times 10^{33})\alpha^{11} - (4.588 \times 10^{23})\alpha^{12} - (5.938 \times 10^{38})\alpha^{13}. \quad (14)$$

The first case considers the pitch response for the flight conditions when $M = 0.75$ and the reduced velocity is $\bar{U} = 1.2$. In order to compare aeroelastic results, time-marching analysis calculations have been evaluated with the same nonlinear curve described by hyperbolic tangent and polynomial, as indicated in Fig. 3.

First, the results are concerned about to check the efficiency of hyperbolic tangent functions to represent continuous polynomial and free-play

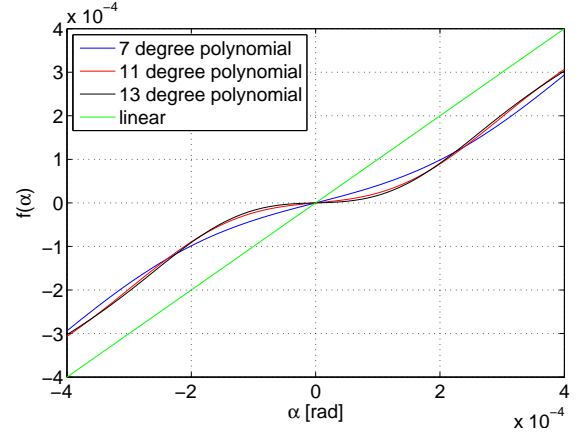


Fig. 2 Structural nonlinearity: 7-degree polynomial, 11-degree polynomial and 13-degree polynomial.

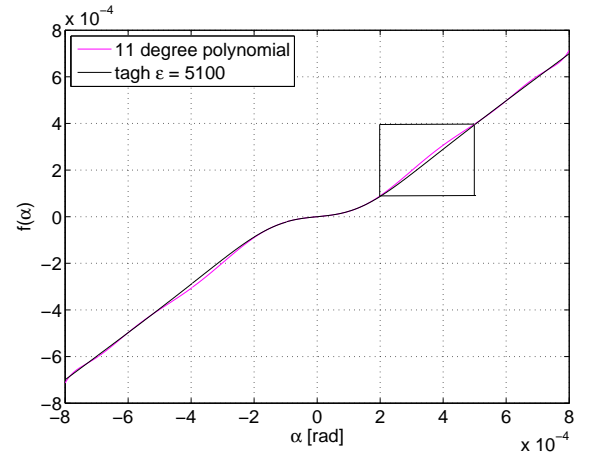


Fig. 3 The same nonlinear curve, P11 and hyperbolic tangent ($\epsilon = 5100$) structural nonlinearity.

structural nonlinearities. Comparisons between the time histories for the P11 polynomial and hyperbolic tangent function for $\epsilon = 5100$ are indicated in Figs. 4 and 5. One can observe from these figures that aeroelastic responses are essentially the same, the system exhibits convergent response. However, different initial behavior in the results are observed, and such behavior seems to be associated to the differences between hyperbolic tangent and polynomial curves. For instance, in the Fig. 3 is indicated a difference between the curves by the square, that correspond the same incidence where initial attractor has been located in aeroelastic response with polynomial nonlinearity (see Fig. 4).

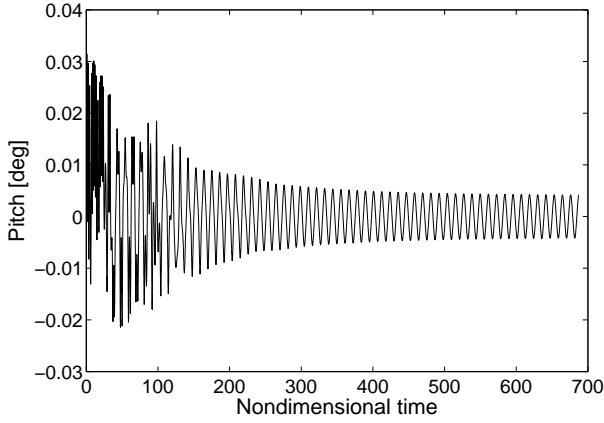


Fig. 4 Time history for $M = 0.75$ and $\bar{U} = 1.2$, P11 structural nonlinearity.

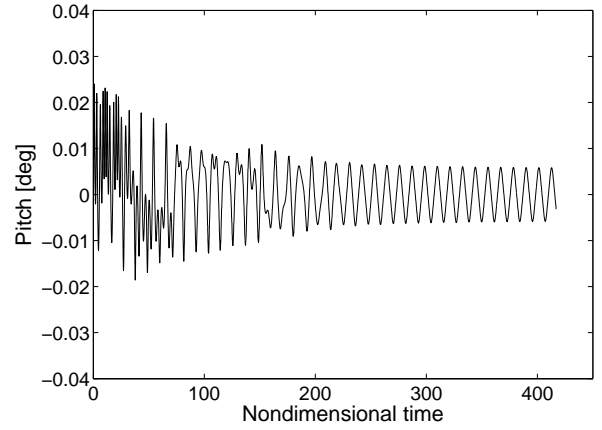


Fig. 6 Time history for $M = 0.75$ and $\bar{U} = 1.2$, P13 structural nonlinearity.

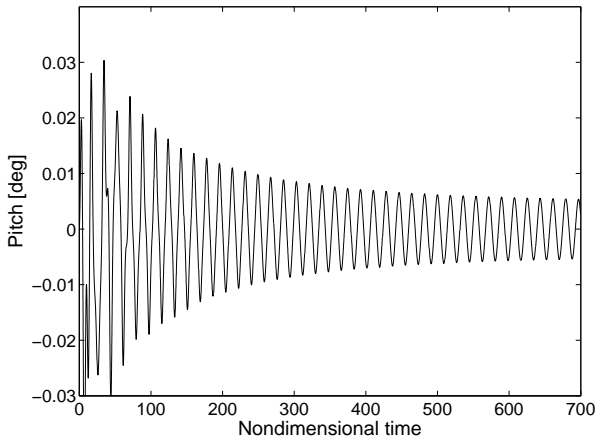


Fig. 5 Time history for $M = 0.75$ and $\bar{U} = 1.2$, hyperbolic tangent ($\epsilon = 5100$) structural nonlinearity.

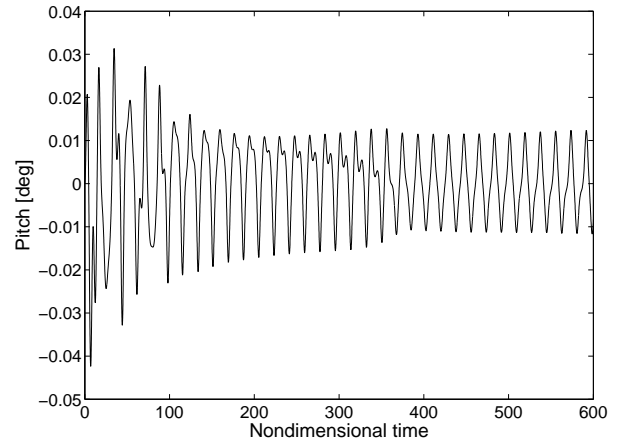


Fig. 7 Time history for $M = 0.75$ and $\bar{U} = 1.2$, hyperbolic tangent ($\epsilon = 6400$) structural nonlinearity.

In order to evaluate aeroelastic behavior with stronger structural nonlinearity, time marching analyses have also been performed for the P13 polynomial and hyperbolic tangent function for $\epsilon = 6400$, indicated in Figs. 6 and 7. As before, these nonlinear functions correspond the same curve. The first aspect that can be checked concerns the fact that these aeroelastic responses show more complex behavior. It can be observed that system, initially, exhibits irregular oscillations and, afterwards, follow somewhat regular oscillations with constant amplitude. The system again shows initial attractor in response with polynomial structural nonlinearity (see Fig. 6).

Finally, the case of free-play is performed for the same flight conditions, *i.e.*, when $M = 0.75$ and $\bar{U} = 1.2$. In this case, the free-play is represented for the hyperbolic tangent function where α_- and α_+ are $\pm 0.005^\circ$. Figures 8 and 9 represent, respectively, time history and phase plane responses with the continuous freeplay nonlinearity in the structure. One can observe that the system exhibits LCO. Comparisons between the aeroelastic responses with structural free-play for the discontinuous representation (Eq. (11)) and hyperbolic tangent representation (Eq. (10)) are evaluated. Time history and phase plane for discontinuous free-play structural model, in the

DYNAMIC ANALYSIS OF AEROELASTIC RESPONSE FOR TRANSONIC FLOW WITH NONLINEAR STRUCTURAL MODEL

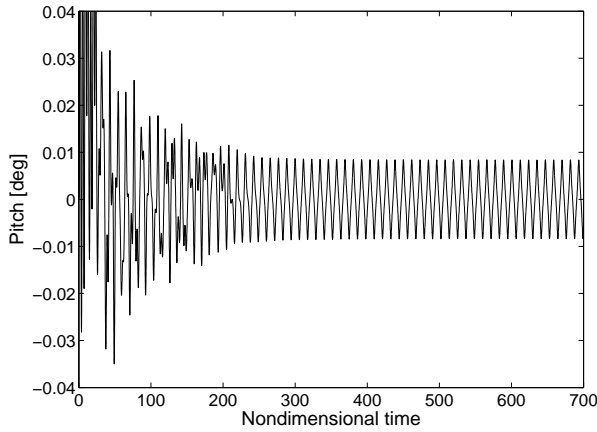


Fig. 8 Time history for $M = 0.75$ and $\bar{U} = 1.2$, hyperbolic tangent free-play structural nonlinearity.

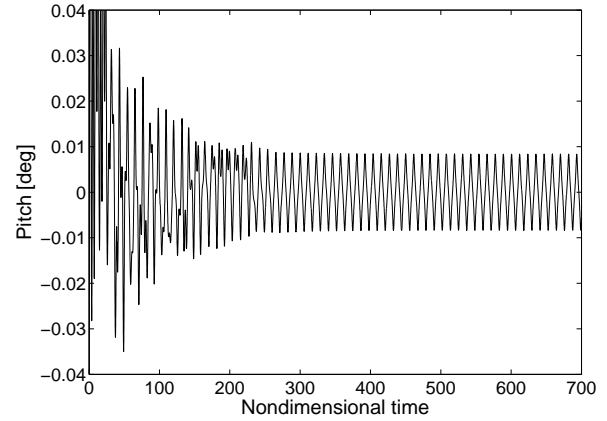


Fig. 10 Time history for $M = 0.75$ and $\bar{U} = 1.2$, discontinuous free-play structural nonlinearity.

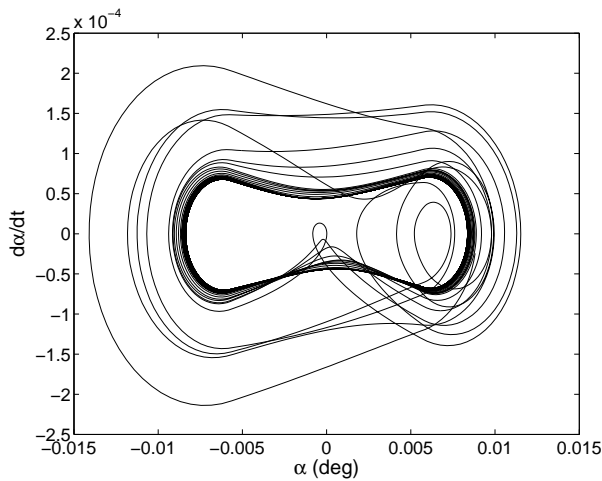


Fig. 9 Phase plane for $M = 0.75$ and $\bar{U} = 1.2$, hyperbolic tangent free-play structural nonlinearity.

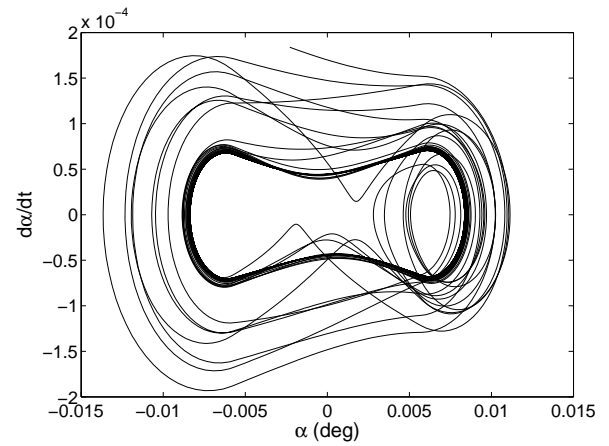


Fig. 11 Phase plane for $M = 0.75$ and $\bar{U} = 1.2$, discontinuous free-play structural nonlinearity.

same flight conditions, are shown in Figs. 10 and 11, respectively. The system behavior is similar that presented with continuous structural free-play, it can be observed when are compared the phase planes in Figs. 9 and 11. Such behavior seems to indicated that discontinuous free-play, in this case, do not show problems with solution accuracy.

The next case considers aeroelastic behavior in flight regime grather than before. Figures 12 to 21 represent the aeroelastic responses for the cases when $M = 0.86$ and the reduced velocity is $\bar{U} = 2.0$. In order to verify the structural

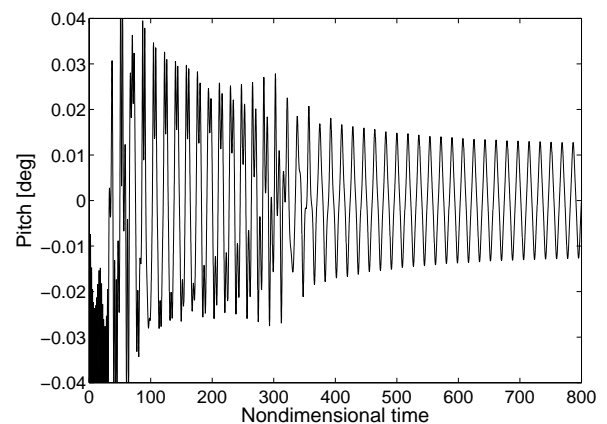


Fig. 12 Time history for $M = 0.86$ and $\bar{U} = 2.0$, P7 structural nonlinearity.

nonlinearities degree in aeroelastic behavior, the polynomial representations has been considered in the model. Figure 12 shows the time history for aeroelastic behavior considering P7 polynomial representation (Eq. (12)), where the result indicate that the latter is convergent response.

Figure 13 shows the time history with the P11 polynomial structural nonlinearity (Eq. (13)). In this case, the system exhibits an LCO type response, however the effect of the nonlinear restoring torsion moment shows strange attractors in the dynamics of the resulting aeroelastic system, as indicated in phase plane in Figure 14. The connection to chaos is inevitable, but chaotic

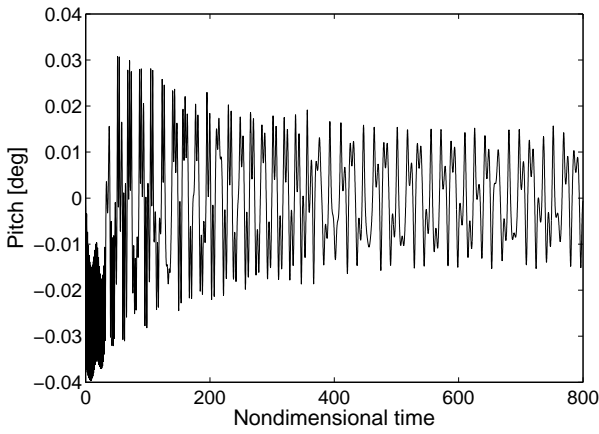


Fig. 13 Time history for $M = 0.86$ and $\bar{U} = 2.0$, P11 structural nonlinearity.

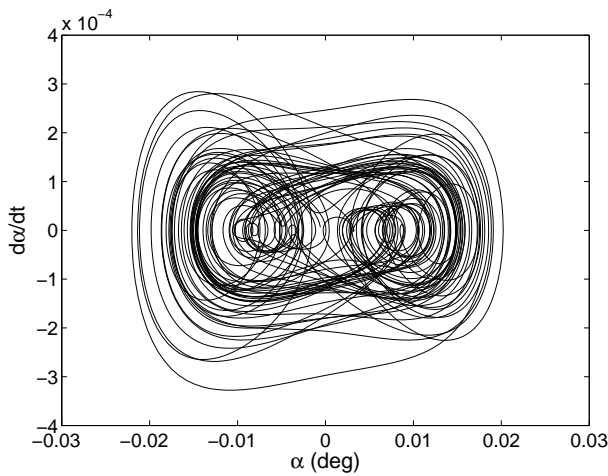


Fig. 14 Phase plane for $M = 0.86$ and $\bar{U} = 2.0$, P11 structural nonlinearity.

behavior is still not well explored and understood as far as aeroelastic systems is concerned. In this case, comparisons between the response for the P11 polynomial and hyperbolic tangent function for $\epsilon = 5100$ are performed. Figures. 15 and 16 show time history and phase plane, respectively. One can observe from phase planes, indicated in Figs. 14 and 16, that aeroelastic responses do not show significant differences. However, the time histories show different initial behavior, as observed in Figs. 13 and 15. As observed before, when $M = 0.75$, such behavior seems to be asso-

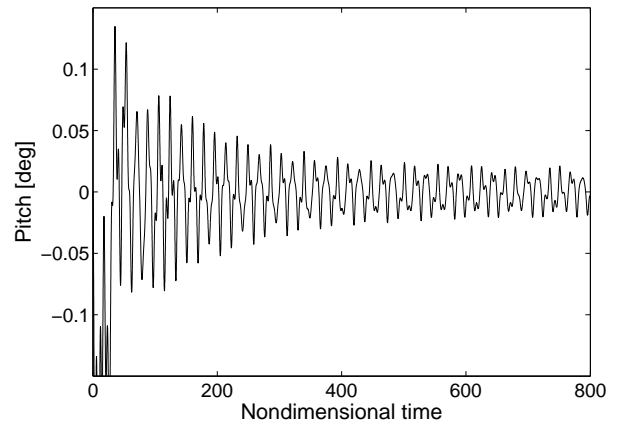


Fig. 15 Time history for $M = 0.86$ and $\bar{U} = 2.0$, hyperbolic tangent ($\epsilon = 5100$) structural nonlinearity.

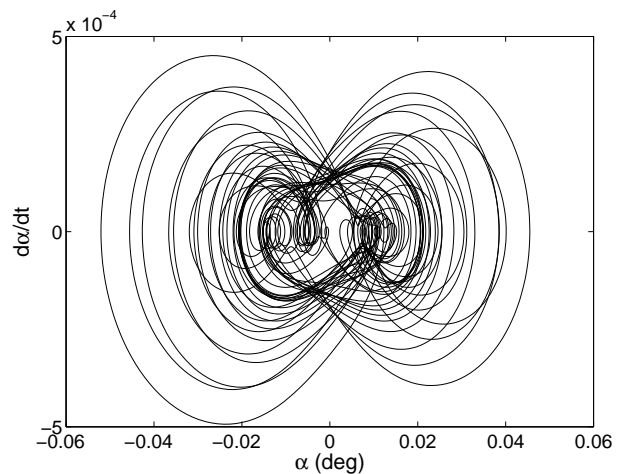


Fig. 16 Phase plane for $M = 0.86$ and $\bar{U} = 2.0$, hyperbolic tangent ($\epsilon = 5100$) structural nonlinearity.

ciated to the differences between hyperbolic tangent and polynomial curves.

Figure 17 shows time history response for P13 structural nonlinearity in the model (Eq. (14)), the system apparently exhibits the same response observed in P11 structural case.

The case of free-play is also performed for this flight conditions, *i.e.*, when $M = 0.86$ and $\bar{U} = 2$. As before, the free-play is represented for the hyperbolic tangent function where α_- and α_+ are $\pm 0.005^\circ$, and $\varepsilon = 5100$. Figures 18 and 19 represent, respectively, time history and phase plane responses with the continuous freeplay nonlinearity in the structure. One

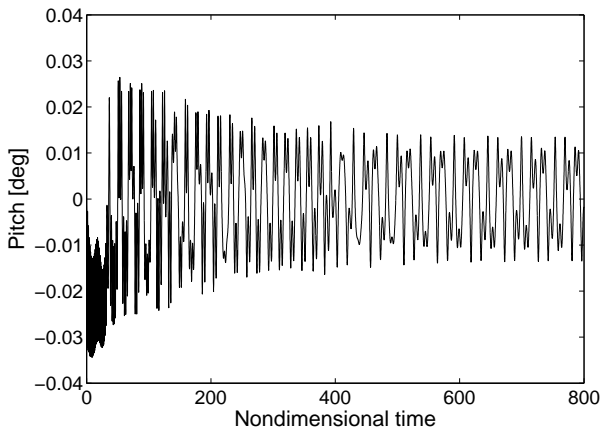


Fig. 17 Time history for $M = 0.86$ and $\bar{U} = 2.0$, P13 structural nonlinearity.

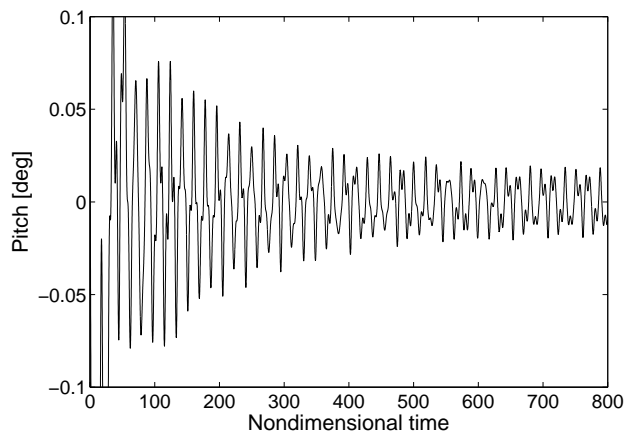


Fig. 18 Time history for $M = 0.86$ and $\bar{U} = 2.0$, hyperbolic tangent free-play structural nonlinearity.

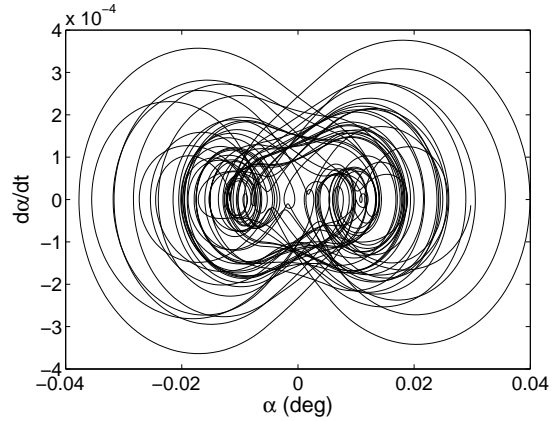


Fig. 19 Phase plane for $M = 0.86$ and $\bar{U} = 2.0$, hyperbolic tangent free-play structural nonlinearity.

can observe that the system exhibits strange attractors in the dynamics of the resulting aeroelastic system. Comparisons between the aeroelastic responses with structural free-play for the discontinuous representation (Eq. (11)) and hyperbolic tangent representation (Eq. (10)) are also evaluated. Time history and phase plane for discontinuous free-play in the structural model are shown in Figs. 20 and 21, respectively. The system behavior is similar that presented with continuous structural free-play, it can be observed when are compared the phase planes in Figs. 19 and 21. As in case of $M = 0.75$ and $\bar{U} = 1.2$, discontinuous free-play seems do not cause problems with solution accuracy when compared with continuous representation in the model.

6 Concluding Remarks

Concentrated nonlinearities are shown to have significant effects on the aeroelastic responses in transonic flow. For the computations performed so far, that typically involve very small incidences, aeroelastic response has presented LCO when a certain degree of nonlinearity is added in the restoring torsion moment. It has been also observed that an increase on degree of the structural nonlinearity the phase plane reveals complex behavior. In the free-play case, the results show the higher effect of structural nonlinearity. However, further analyses are still necessary in or-

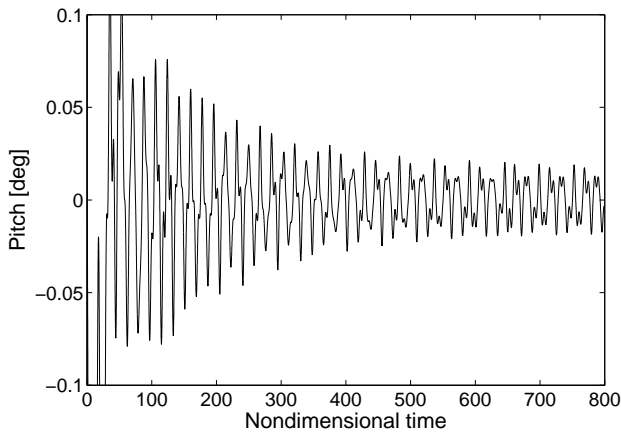


Fig. 20 Time history for $M = 0.86$ and $\bar{U} = 2.0$, discontinuous free-play structural nonlinearity.

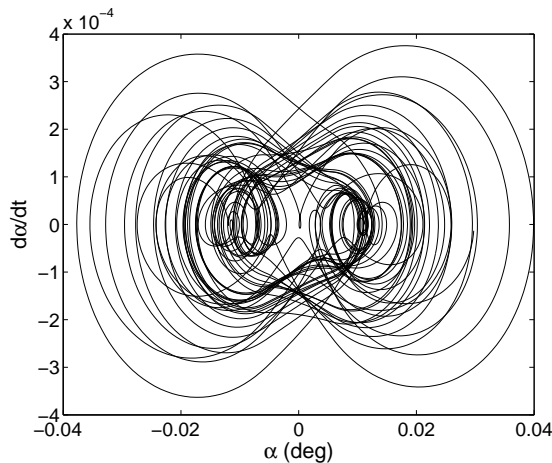


Fig. 21 Phase plane for $M = 0.86$ and $\bar{U} = 2.0$, discontinuous free-play structural nonlinearity.

der to characterize the complete behavior of such nonlinear systems.

The detailed comparison of hyperbolic tangent and polynomial nonlinearities reveal a good approximation between these representation of the curves in the aeroelastic solutions. Results of discontinuous free-play nonlinearity have not been shown significant differences in the responses for those cases with continuous representation of free-play. However, continuity is a necessary condition to guarantee accurate solutions with the Runge-Kutta method employed in the present work. The next step is to apply such torsional polynomial nonlinearity in the structure for the Hopf Bifurcation analysis to check which terms of

the polynomial influence the flutter boundary.

7 Acknowledgements

The authors acknowledge the financial support of the Brazilian Federal Research Agency, *CNPq*.

References

- [1] Oliveira, L. C., "A state-space aeroelastic analysis methodology using computational aerodynamics techniques", Master Thesis - Instituto Tecnológico de Aeronáutica, São José dos Campos, S. P., Brazil, 1993 (in Portuguese).
- [2] Simões, C. F. C.; Azevedo, J. L. F., "The influence of numerical parameters on unsteady airfoil inviscid flow simulations using unstructured dynamic meshes", Brazilian Progress in Aerospace Engineering, Águas de Lindóia, São Paulo, Brazil, 22-26 Nov 1999.
- [3] Liu, F.; Cai, J.; Zhu, Y.; Tsai, H. M. and Wong, A. S. F., "Calculation of wing flutter by a coupled fluid-structure method", *Journal of Aircraft*, vol. 38, n. 2, pp. 334-342, Mar-Apr 2001.
- [4] Morton, S. A.; Beran P. S., 1999, "Hopf-Bifurcation Analysis of Airfoil Flutter at Transonic Speeds", *Journal of aircraft*, vo. 36, n. 2.
- [5] Badcock, K. J.; Woodgate, M. A.; Richards, B. E., "Hopf Bifurcation Calculations for Symmetric Airfoil in Transonic Flow", *AIAA Journal*, vol. 42, n. 5, pp. 883-892, May 2004.
- [6] Badcock, K. J.; Woodgate, M. A.; Richards, B. E., "Direct Aeroelastic Bifurcation Analysis of a Symmetric Wing Based on Euler Equations", *Journal of Aircraft*, vol. 42, n. 3, May-June 2005.
- [7] Alonso, J. J. and Jameson, A., "Fully-implicit time-marching aeroelastic solutions", 32nd AIAA, Aerospace Sciences Meeting & Exhibit, 32nd, Reno, NV, 10-13 January 1994.
- [8] Kousen, K. A. and Bendiksen, O. O., "Limit cycle phenomena in computational transonic aeroelasticity", *Journal of Aircraft*, vo. 32, n. 2, pp. 1257-1263, 1994.
- [9] Thomas, J. P. and Dowell, E. H. and Hall, K. C., "Nonlinear inviscid aerodynamic effects on transonic divergence, flutter, and limit-cycle oscillations", *AIAA Journal*, vol. 40, n. 4, pp. 638-646, 2002.

- [10] Camilo, E. ; Marque, F. D. ; Azevedo, J. L. F., 2006, "Aeroelastic analysis of typical sections with structural and aerodynamic nonlinearities". *In: 25th International Council of the Aeronautical Sciences – ICAS 2006*, Hamburgo – Alemanha.
- [11] Camilo, E. ; Marques, F. D. ; Azevedo, J. L. F., 2007, "Time-marching aeroelastic analysis of typical sections with structural nonlinearities in transonic regime". *In: 12th International Symposium on Dynamic Problems of Mechanics – DINAME 2007*, Ilha Bela – SP – Brazil.
- [12] Ko, J. and Kurdila, A. J. and Strganac, T. W., "Nonlinear dynamics and control for a structurally nonlinear aeroelastic system", Published by the American Institute of Aeronautics and Astronautics, 1997.
- [13] Conner, M. D.; Virgin, L. N. and Dowell, E. H., "Accurate numerical integration of state-space models for aeroelastic systems with free-play", *AIAA Journal*, vol. 34, n. 10, pp. 2202-2205, 1996.
- [14] Henon, M., "On the numerical computation of Poincaré maps", *Physica D*, vol. 5, pp. 412-414, 1982.
- [15] Jones, D. P.; Roberts, I. and Gaitonde, A. L., "Identification of limit cycles for piecewise nonlinear aeroelastic system", *Journal of Fluid and Structures*, vol. 23, n. 7, pp. 1012-1028, 2007.
- [16] Azevedo, J.L.F., "On The Development of Unstructured Grid Finite Volume Solver for High Speed Flows", *Report NT-075-ASE-N/92*, Instituto de Aeronáutica e Espaço, São José dos Campos, SP, Brazil, 1992.
- [17] Jameson, A. and Schmidt, W. & Turkel, E., "Numerical simulation of the euler equation by finite volume using Runge-Kutta time stepping schemes", *AIAA Paper*, pp. 81-1259, 1981.
- [18] Bisplinghoff, R. L.; Ashley, H. and Halfman, R. L., "Aeroelasticity", Dover – New York, 1996.
- [19] Lee, B. H. K. and Price, S. J. and Wong, Y. S., "Nonlinear aeroelastic analysis of airfoils: bifurcation and chaos", *Progress in Aerospace Sciences*, Vol.35, pp. 205-334, 1999.

7.1 Copyright Statement

The authors confirm that they, and/or their company or institution, hold copyright on all of the original material included in their paper. They also confirm they have obtained permission, from the copyright holder of any third party material included in their paper, to publish it as part of their paper. The authors grant full permission for the publication and distribution of their paper as part of the ICAS2008 proceedings or as individual off-prints from the proceedings.